ACS Partner Journal

CHEMICAL & BIOMEDICAL IMAGING

pubs.acs.org/ChemBioImaging

Letter

In Situ Electrochemical Monitoring of *Bacillus cereus* Biofilm Formation

Published as part of Chemical & Biomedical Imaging special issue "Electrochemistry and Imaging".

Aleksandar Mijajlovic, Dalibor Stankovic, Milica Sentic, Vlad Costache, Shanshan Wang, Hadi Jbara, Julien Deschamps, Romain Briandet, Neso Sojic, and Jasmina Vidic*

Cite This: https://doi.org/10.1021/cbmi.5c00271

Read Online

ACCESS | Metrics & More | Article Recommendations | Supporting Information

ABSTRACT: Unwanted biofilms pose significant challenges in the food industry, on medical devices, in water supply systems and marine environments, and even in space exploration. Label-free, advanced sensing approaches such as electrical impedance spectroscopy (EIS) have been investigated as tools for monitoring biofilm formation. The electrode material and the surrounding medium, differing in carbon source, ionic strength, or nutrient availability, can strongly influence bacterial metabolic activity, extracellular polymeric substance (EPS) production, and consequently the resulting impedimetric parameters. Here, we report *Bacillus cereus* (*B. cereus*) biofilm formation on gold and indium tin oxide (ITO) surfaces in two bacterial media that promote biofilm formation. We characterized the impedance responses of biofilms formed at different time points after inoculation and demonstrated a direct correlation between variations in charge transfer resistance and biofilm structure. Non-Faradaic EIS, confocal laser scanning microscopy, and scanning electron microscopy all indicated that *B. cereus* exhibited faster biofilm development on ITO than on gold, possibly due to differences in surface charge or antibacterial effects associated with the nanostructured gold surface. We demonstrate a strong correlation between EIS measurements and microscopic imaging observations of early biofilm formation and the extent of biofilm development. This combination of methodologies provides a reliable approach for detecting and characterizing biofilms, particularly given the high heterogeneity and dynamic behavior of microbial communities.

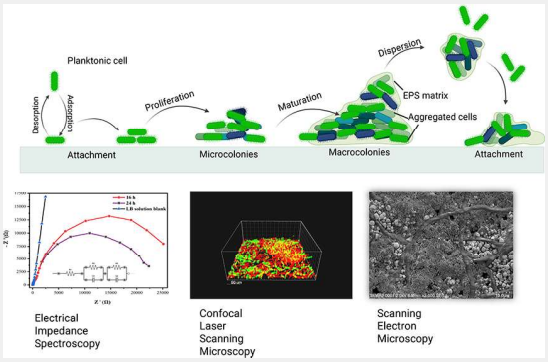

KEYWORDS: *Bacillus cereus, Electrical impedance spectroscopy, Bacterial biofilm, Confocal laser scanning microscopy, Scanning electron microscopy, Extracellular polymeric substance*

Bacterial species of the *B. cereus* group are widespread in the environment and include both probiotic and pathogenic strains associated with infections in humans.[1] The adaptation of bacteria to harsh conditions is strongly marked by phenotypic alterations and biofilm formation which, alongside spores, are the basis for bacterial persistence. Biofilms contribute to the bacterial substantial resistance to environmental stresses and their strong capacity to adhere to a variety of abiotic surfaces, including stainless steel, widely used in food-processing facilities or even living tissues. *B. cereus* biofilms represent a significant concern in clinical settings and industries that demand sterility such as the food industry and pharmaceutical manufacturing.[1−4] Within these settings, *B. cereus* biofilms can persist for long periods and may withstand routine sanitization procedures.

B. cereus cells can differentiate into distinct functional states, including sporulating, competent, motile, and cannibal phenotypes, and can also synthesize a variety of extracellular polymeric substances such as the lipopeptide surfactin, biofilm matrix polysaccharides, nucleic acids, lipids, teichoic acids, and proteins.[5−7] These properties enable the bacterium to efficiently form complex multicellular communities of biofilms in which bacterial cells are embedded within the EPS matrix and protected from the environment. The sessile, biofilm-embedded cells, confers upon bacteria a marked resistance to chemical fluctuations in their microenvironment, a stark contrast to the vulnerability of planktonic cells. This resilience hinders the penetration of antimicrobial agents and immune system components, making bacterial eradication exceptionally difficult and often impossible.

In the majority of *B. cereus* isolates, biofilms typically appear as floating pellicles, though they can also adhere to submerged

Received: December 23, 2025
Revised: February 2, 2026
Accepted: February 4, 2026

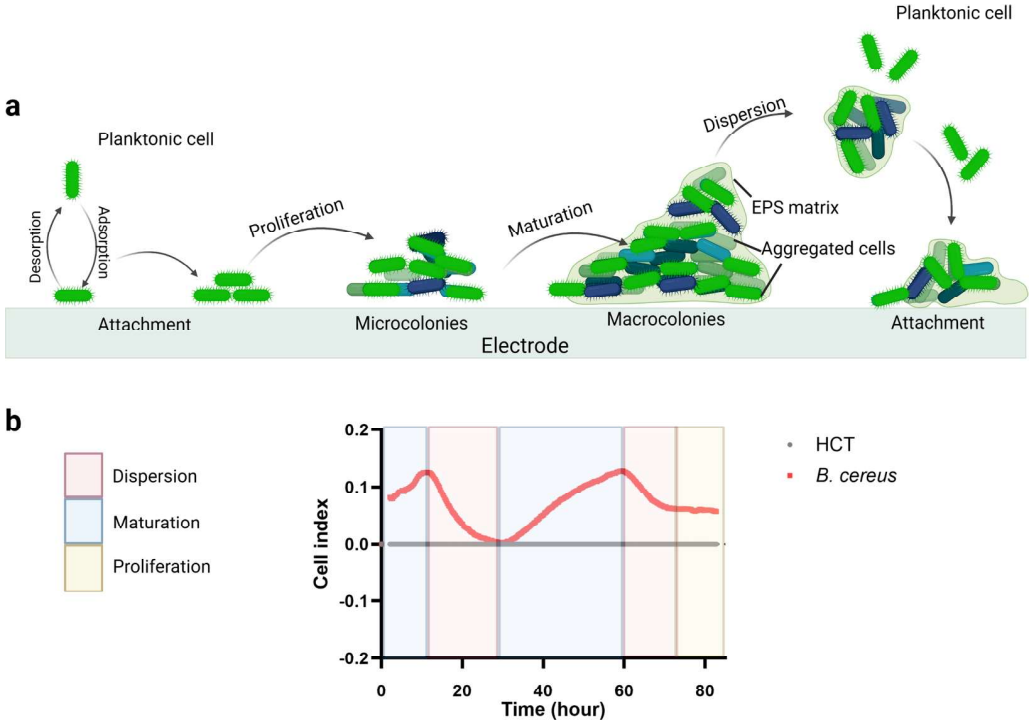

Figure 1. *B. cereus* biofilm life cycle. (a) Schematic illustration of phenotypically distinct stages (attachment, maturation, and dispersal) of bacterial biofilm. (b) *B. cereus* biofilm development for an 80 h time frame in the HCT medium was monitored using xCELLigence assay and E-Plates 16. The cell index was monitored from repeated experiments (n = 3).

surfaces. Like in most bacteria, the development of *B. cereus* biofilm is a cyclic process marked by phenotypically distinct stages: initial attachment, maturation, and dispersal (Figure 1a). The growth and development of biofilms involve a complex array of physiochemical mechanisms, making their timely detection and characterization critical for developing effective prevention and mitigation strategies.[8] Despite the importance of biofilms in microbiology, methods to monitor them are underdeveloped. Traditional detection often relies on indirect, culture-based techniques such as plate counting, tube methods, and microtiter plate assays.[9,10] While routine, these methods are limited by their dependence on the ability to culture sampled cells. To overcome these limitations, a range of advanced techniques is employed. Nucleic acid–based methods, such as polymerase chain reaction and reverse transcription polymerase chain reaction, are used to determine the genetic composition of a biofilm.[4] Imaging plays a vital role in visualizing biofilm architecture and dynamics. Techniques such as light, electron, and confocal microscopy are commonly used, often in conjunction with dyes or fluorescent tags to resolve complex 3D structures.[11] Finally, advanced analytical approaches, including quartz crystal microbalance,[12] surface plasmon resonance[13] and surface-enhanced Raman spectroscopy,[14] offer sensitive, label-free methods for detecting and analyzing biofilms. However, these methods are powerful for studying early stage biofilm attachment and surface interactions, but have limitations in monitoring thick or mature biofilms.

Although current methods remain valuable for studying and understanding biofilms, there is a growing need for real-time evaluation approaches to better address the various aspects of biofilm development and removal. Impedance spectroscopy is an emerging noninvasive technique for biofilm detection and characterization that can not only monitor the complex and adaptive nature of microbial biofilms but also support their cultivation under specific conditions.[10] Impedimetric sensors measure changes in electrical impedance between two electrodes exposed to a bacterial culture. As bacteria and their EPS components act as dielectric materials, they alter the overall impedance signal.

Here, we combined reagent-free electrical impedance spectroscopy with microscopy techniques to monitor *B. cereus* biofilm life cycle at the liquid–solid interfaces using a gold and indium tin oxide electrode materials. By tracking changes in resistance, capacitance, and impedance over time, we can deduce bacterial growth, biofilm formation, and subsequent shifts in biofilm composition and metabolic activity in real time. A key advantage of this electrochemical approach is its high sensitivity, which allows it to capture both the initial adhesion of cells to a surface and the production of EPS containing specific electroactive species. Results of electrochemical sensing are correlated with observations of biofilm biomass using confocal laser scanning microscopy (CLSM) and scanning electron microscopy (SEM).

To determine the time scale of *B. cereus* biofilm formation on a gold surface, we allowed bacterial cells to adhere to gold microelectrodes associated with the bottom of wells of microtiter plate (well bottom diameter 5.0 ± 0.075 mm), washed wells to remove nonadherent cells, and performed the xCELLigence impedimetric assay in the electrically conductive solution HCT (growth medium which favorizes biofilm formation of *B. cereus*).[15] In this assay, bacterial cells are exposed to a nondestructive voltage in an intermittent way and the cell index, a dimensionless unit, is calculated as a relative change in electrical impedance compared to the background impedance.[16] A control microelectrode in contact with the HCT medium alone showed a weak cell index signal due to an easy

https://doi.org/10.1021/cbmi.5c00271
Chem. Biomed. Imaging XXXX, XXX, XXX–XXX

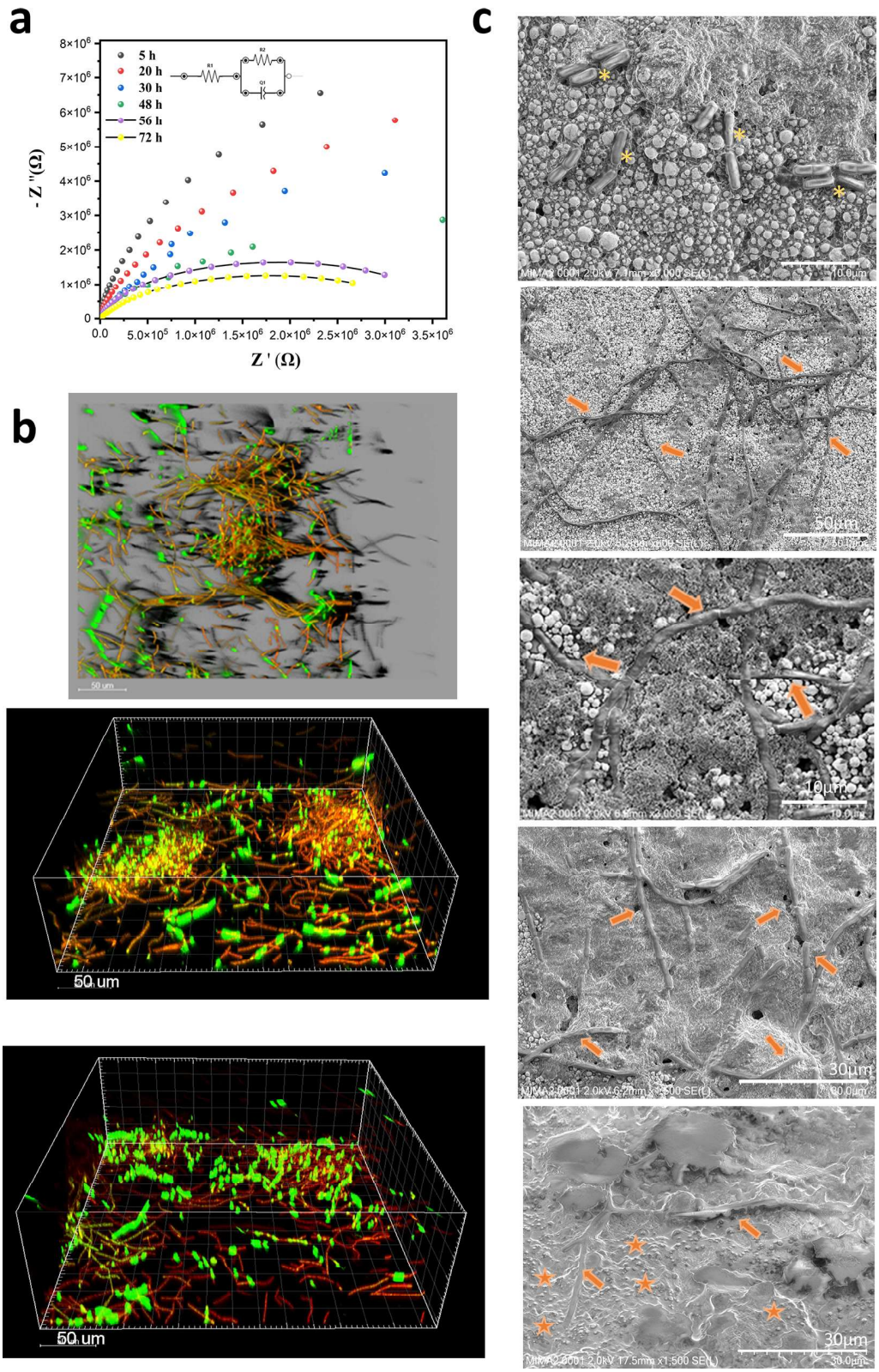

Figure 2. *B. cereus* biofilm on a gold electrode. (a) Representative impedance spectra for *B. cereus* showing the imaginary impedance ($-Z''\Omega$) plotted as a function of the real impedance ($Z'\Omega$) recorded at indicated times after inoculation. The solid lines represent fitting curves, while the experimental results are shown with dots. EIS parameters: frequencies ranged from 0.01 Hz to 100 kHz; amplitude, 10 mV. (b) 24 h biofilm stained with a live/dead stain and imaged using confocal laser scanning microscopy. The upper image shows a top-down view of an image stack, while the lower images display IMARIS-processed 3D images of live and dead cells. All three images were taken from different locations on the electrode. (c) 24 h biofilm visualization using scanning electron microscopy. Asterisks indicate planktonic cells, arrows indicate fiber-like structures, and stars indicate spores embedded within the biofilm.

https://doi.org/10.1021/cbmi.5c00271
Chem. Biomed. Imaging XXXX, XXX, XXX−XXX

movement of ions under the applied electrical field, resulting in low impedance changing (Figure 1b). In contrast, the microelectrode with adhered *B. cereus* cells showed a rapid increase of impedance over time indicating the proliferation of the attached cells and the matrix production on the gold surface (Figure 1b). The resulting cell index reached plateau at 12 h, after which decreased due to the detachment of the biofilm. The detached portion of the biofilm started to grow again at 32 h, leading to a new resistance increase (Figure 1b). Within this new cycle, the biofilm continued to maturate, and reached a new plateau at 60 h postinoculation. At approximately 72 h a new large detachment was observed as reflected in a decrease in impedance intensity. These findings suggest that the maturation/detachment cycle of *B. cereus* biofilm on gold surfaces takes from 25 to 30 h.

We then applied EIS to thoroughly characterize *B. cereus* biofilm formation on an electrode surface. In contrast to xCELLigence which relies on single-frequency impedance measurements summarized as a Cell Index, EIS provides frequency-resolved, model-based analysis that enables the extraction of specific biophysical parameters.[17] Small-amplitude sinusoidal electrical disturbances were applied to biofilms attached to electrodes (10−20 mV), with the frequency varying over several orders of magnitude (0.01 Hz to 100 kHz) and the resulting complex frequency-domain electrical responses were analyzed to provide information on electrochemical processes.[18−20] These parameters were selected to optimize the signal-to-noise ratio and to capture both high-frequency interfacial processes and low-frequency diffusion-related phenomena characteristic of biofilm−electrode systems. The method is widely used in materials electrochemistry, and its application in monitoring biofilms and microbial corrosion is well established.[21,22]

The activated and sterilized surface of the screen-printed gold electrode (SPGE) was incubated with *B. cereus* planktonic cells and rinsed to remove nonattached bacterial cells. The electrode was then incubated with HCT medium within a homemade three-electrode electrochemical cell, and the impedance was measured over time. EIS results presented in Figure 2a show Nyquist plots (imaginary vs real component) of *B. cereus* biofilm formation on an SPGE. The non-Faradaic EIS spectra were stable and reproducible over the entire frequency range. The plots indicate a steady decrease in the diameter of the impedance arc with incubation time from 5 to 72 h, reflecting the growth and maturation of the biofilm during this time period. As expected, when only few bacterial cells were attached to the electrode surface, the semicircle was large (Figure 2a, at 5 h), indicating a high charge transfer resistance (R_{ct}). The R_{ct} can be resumed as a contact resistance between the electrode and the biofilm, and its high values suggest the compact coverage of the electrode giving the electron transfer between the electrode surface and the electroactive species in solution intrinsically inefficient. Overtime, the cell proliferation and the EPS production decreased R_{ct} (Figure 2a). At 72 h, the semicircle is significantly smaller, due to the biofilm that acts as a kinetic barrier, slowing electron tunneling and raising R_{ct}.

Between 30 and 72 h, the R_{ct} decreases, indicating that electrons can move more easily across the electrode−solution interface over time (Figure 2a). This suggests that the dielectric or conductive properties of the biofilm on the electrode are changing as it matures. This may occur because a mature biofilm becomes denser and more hydrated, contains more redox-active molecules, or forms a more electronically conductive matrix. Similarly, it was previously shown that during the first 24−72 h of *Escherichia coli* (*E. coli*) biofilm growth, the formation of conductive channels within the biofilm and a closer contact between cells and the electrode surface led to enhanced in charge transfer efficiency.[23] The overall decrease in impedance observed between 5 and 72 h therefore indicates that the *B. cereus* biofilm evolves from an insulating to an electroactive and conductive layer, improving electron exchange and reducing interfacial resistance. This information cannot be extrapolated from the xCELLigence assay, which cannot distinguish between resistance and capacitance components.

Indeed, the accumulation of EPS and metabolically active bacterial cells makes the biofilm thicker, denser, and more structured, which facilitated electron and ion transport, and thus decreased *R*.[24] The results obtained show that biofilm growth on a SPGE is extremely challenging. Only the spectra obtained after 56 and 72 h could be properly fitted, yielding an R_{ct} of $(3.8 \pm 0.573) \times 10^6\ \Omega$ and $(2.6 \pm 0.0832) \times 10^6\ \Omega$, respectively. The higher dispersion (32%) observed for mature biofilms on gold at 72 h suggests biofilm heterogeneity and detachment. Figure 2a inset depicts the equivalent circuit, which includes the solution resistance in series (R_1), a parallel combination of the charge-transfer resistance (R_2), and a constant-phase element representing the double-layer capacitance (Q_1). This circuit accurately describes the interfacial charge-transfer behavior observed during prolonged biofilm maturation durations. The spectra obtained for incubation times shorter than 56 h showed nonideal behavior, preventing accurate fitting.

In contrast to the *B. cereus* life cycles observed on gold microelectrodes in the xCELLigence assay, when the first mature biofilm was formed after only 12 h (Figure 1b), the bacterium on the SPGE started to form compact biofilm only after 48 h (Figure 2a). To verify whether *B. cereus* adheres and forms multicellular communities on gold, the three-dimensional structure of 24 h biofilms formed on the SPGE with high resolution fluorescence imaging was analyzed using CLSM. Before acquisition, biofilms were stained with fluorescent DNA-binding dyes SYBR-Green and propidium iodide (PI), using LIFE/DEAD BacLight Kit.[25] The results confirmed the ability of *B. cereus* to form biofilms on the gold surface (Figure 2b), and revealed a surface-associated community with marked structural heterogeneity, protuberant structures that could reach a height of more than 20 μm, as shown in 3D images at the bottom of Figure 2b.

Micrographs of the biofilm revealed the organized formation of cell aggregates, clusters, and microcolonies (Figure 2c). This finding is in accordance with the high R_{ct} measured at this time scale. The majority of live bacterial cells (stained by SYBR Green that binds to intercellular DNA) were located at the top of the biofilm, indicating that most metabolic activity occurs in this region (Figure 2b). In contrast, PI-stained extracellular DNA and dead cells were mainly attached to the electrode surface, where they formed fiber-like structures.

The scanning electron microscopy visualization of 24 h old biofilms confirmed that the electrode surface was not completely covered (Supporting Information Figure S2). Deeper SEM analysis indicated that biofilm grew only within bacterial microcolonies and a patchy distribution of EPSs, as shown in Figure 2c. Three main structural organizations were observed: (i) isolated planktonic cells that probably originated from dispersion of the biofilm, (ii) fibril-like structures, and (iii) compact biofilms that contained dense EPS, amyloid-like structures and numerous spores (Figure 2c). Many *Bacillus*

https://doi.org/10.1021/cbmi.5c00271
Chem. Biomed. Imaging XXXX, XXX, XXX−XXX

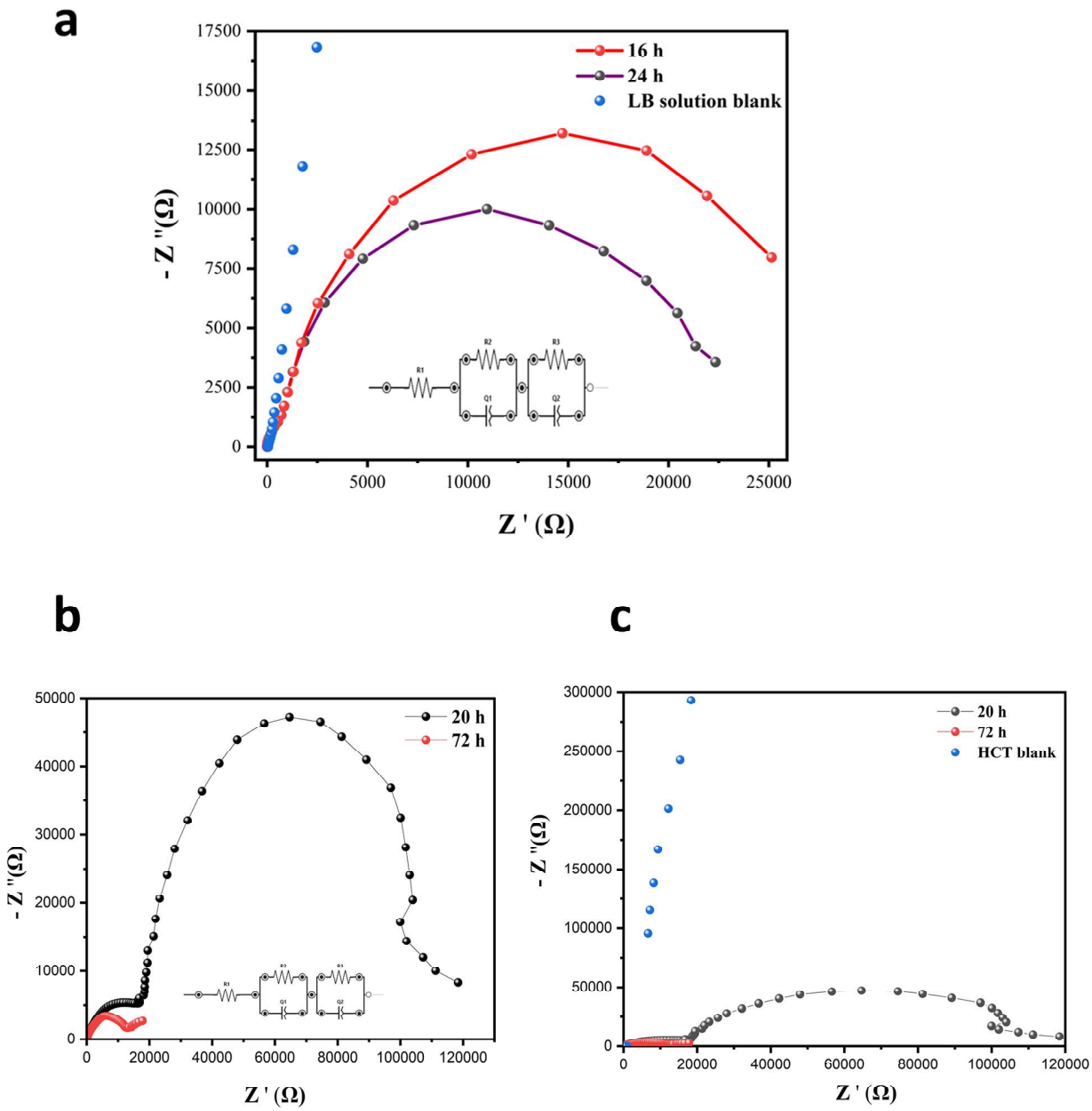

Figure 3. Variation of non-Faradaic EIS spectra of *B. cereus* as a function of growth time. (a) Nyquist plots of *B. cereus* biofilm recorded in LB medium at different incubation times. The inset presents the equivalent circuit model used to fit the experimental data. (b) Impedance spectra of 20 and 72 h biofilm in the HCT medium with the corresponding equivalent circuit model (inset). (c) Comparison of impedance responses for biofilm (20 and 72 h) with the HCT medium without biofilm (blank). The solid lines represent fitting curves, while the experimental results are shown with dots. EIS parameters: frequencies ranged from 0.01 Hz to 100 kHz; amplitude, 20 mV.

species, including *B. cereus* and *B. subtilis*, produce amyloid-like proteinous fibers and eDNA that enhanced mechanical strength and persistence of the community.[26]

These fibrillar EPS structures participate in the spatial architecture of the biofilm, and the coordination of multicellular behavior. Considering that fibrillar structures act as physical connectors, strengthening the 3D biofilm matrix, their presence suggests that *B. cereus* adhesion to the gold surface requires bacterial metabolic and phenotypical adaptation.[3] Moreover, bacterial sporulation within biofilms (indicated by stars in Figure 2c) shows that the gold environment triggers stress signals that promote spore formation within biofilms as an adaptive survival strategy.[3]

Next, *B. cereus* biofilm growth was assessed using ITO electrodes. These electrodes, having optical transparency, electrical conductivity, and structural uniformity, provide ideal surfaces for simultaneous microscopic and electrochemical monitoring.[27−29] In situ biofilm formation at the ITO was followed in LB and HCT media to elucidate the effects of nutritional conditions on biofilm structure and electrochemical properties. To separate the intrinsic effect of the growth medium from that of the biofilm, control experiments were performed with the bare electrode immersed in each medium (Figure 3).

For the LB medium, EIS experiments were performed at a DC potential of 0 V, with an AC amplitude of only 10 mV and a frequency range from 0.2 Hz to 100 kHz, to maintain the

https://doi.org/10.1021/cbmi.5c00271
Chem. Biomed. Imaging XXXX, XXX, XXX−XXX

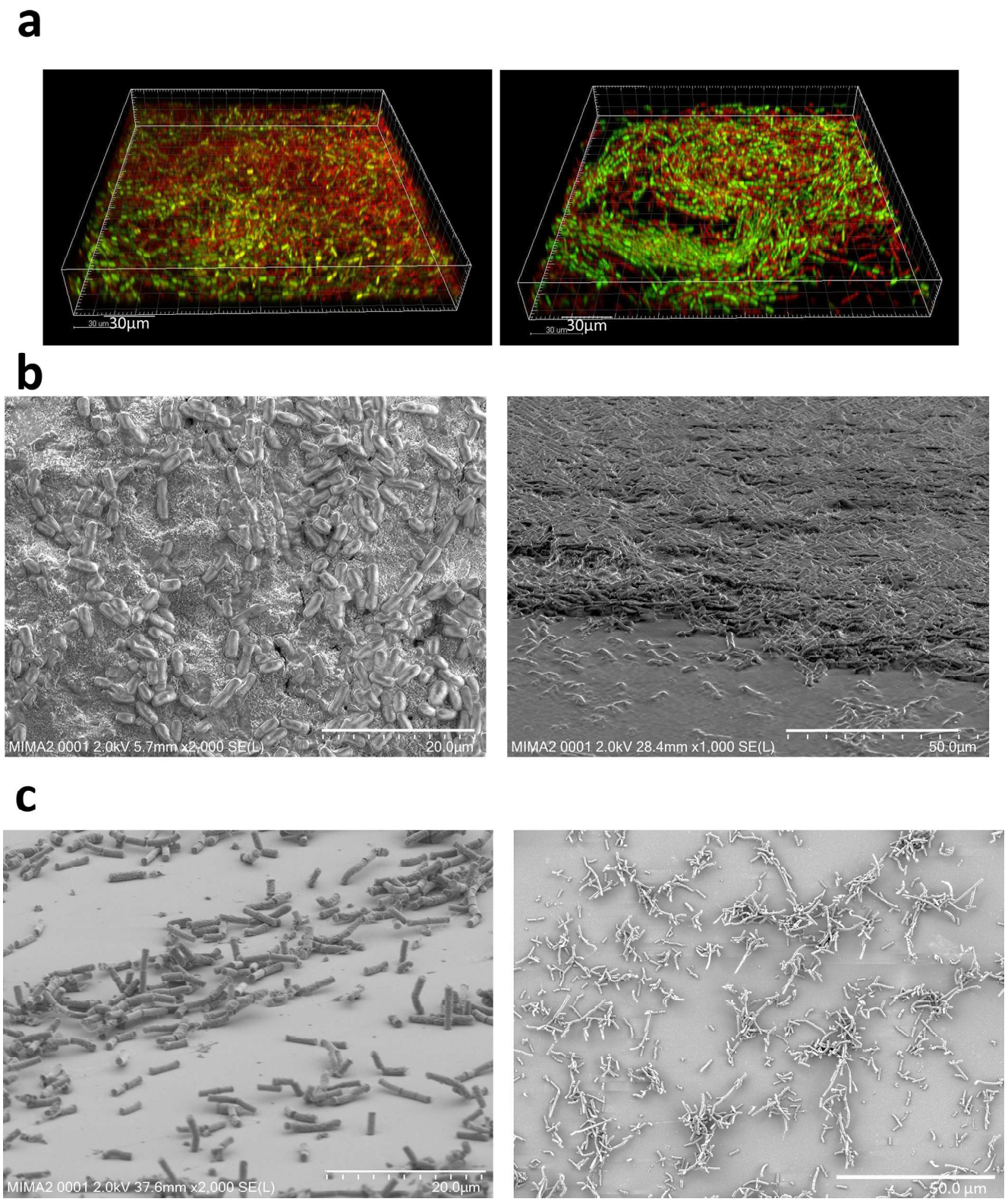

Figure 4. Microscopic visualization of *B. cereus* biofilm on an ITO electrode 24 h after inoculation. (a) IMARIS processed 3D CLMS images of live and dead volumes of *B. cereus* biofilm. (b) Biofilms formed on the ITO were imaged directly by SEM under high-vacuum conditions, without prior fixation or dehydration. (c) ITO surface visualization by SEM after biofilm fixation. The biofilm preparation (aldehyde fixation and dehydration) disrupted the EPS matrix and some of the bacteria but allowed better observation of cell morphology.

attached cell health (Figure S1). The Nyquist plots obtained are presented in Figure 3a. With both 16 h and 24 h biofilms, two distinct semicircles are observed, indicating the presence of the compact biofilm and at least two separate electrochemical processes occurring at the biofilm−electrode interface. The equivalent circuit model that provided the best fit to the

https://doi.org/10.1021/cbmi.5c00271
Chem. Biomed. Imaging XXXX, XXX, XXX−XXX

experimental data is shown as an inset in Figure 3a. The circuit consists of a series resistance (R_1) connected to two parallel R–Q elements (R_2–Q_1 and R_3–Q_2), each representing distinct electrochemical processes occurring at the biofilm–electrode interface. In this configuration, R_1 corresponds to the solution resistance, which accounts for the ionic resistance of the LB medium between the reference and the working electrode. The elements R_2 and R_3 represent the R_{ct} associated with two different interfacial processes or biofilm layers. Each of these resistances is coupled with a constant phase element, denoted as Q_1 and Q_2, to describe the nonideal capacitive behavior of the system, arising from surface heterogeneity, biofilm roughness, and distributed charge storage effects. The presence of two R–Q branches indicates that the system exhibits two distinct time constants, corresponding to electrochemical processes occurring at different depths of the biofilm. The first branch (R_2–Q_1) can be attributed to the outer, more electroactive region of the biofilm, where faster charge transfer occurs, while the second branch (R_3–Q_2) represents the inner, diffusion-limited layer, where mass transport and redox reactions are slower.[23,30,31] Of these, R_{ct} and constant phase element (CPE) depend on the dielectric and insulating features at the electrode–biofilm interface, and are controlled by modifying the electrode's surface. The fitting parameters showed that there was only a very slight change of CPE with biofilm maturation, the major change being a decrease of the charge transfer resistance R_{ct}. The R_{ct} value after 16 h was 25413 ± 3360 Ω, while after 24 h it decreased to 22366 ± 3090 Ω. This decrease indicates a recovery in the efficiency of the mass transfer phenomenon and/or a difference in the dielectric or conductive properties of the bacterial cell organization and EPS production on the electrode surface due to the biofilm maturation.

In the case of the HCT medium, the measurements on the ITO were conducted at the same potential of 0 V, but with an AC amplitude of 20 mV and a frequency range of 0.001 Hz to 1 kHz. The purpose was to emphasize the long-term electrochemical evolution of the biofilm, from the intermediate stage of active growth (20 h) to the late, stabilized phase (72 h). Similar electrochemical behavior was observed in both HCT and LB medium, as shown in Figure 3b,c. The corresponding equivalent circuit model used to fit the data is shown as an inset in Figure 3b. At 72 h, the diameter of the semicircle is significantly smaller than that recorded at 20 h demonstrating a clear decrease in R_{ct} at prolonged biofilm growth. Converting the obtained conclusion into numerical comparison, the R_{ct} after 20 h was 118500 ± 11600 Ω, whereas after 72 h it decreased drastically to 12918 ± 2150 Ω—approximately nine times lower. This suggests that the biofilm evolved from a heterogeneous, partially insulating layer into a more electroactive and conductive structure, reflecting its progressive maturation and improved electron transfer efficiency. As with the LB medium (Figure 3a), control measurements using bare ITO electrodes immersed in HCT medium (Figure 3c) confirmed that the observed differences in the impedance spectra originated primarily from the biofilm rather than from variations in the bulk electrolyte conductivity. The comparison between the "bare electrode + medium" and "biofilm + medium" conditions demonstrates that the impedance changes arise from biofilm formation and not from the inherent conductivity of the electrolyte.

The EIS results indicate that a more developed biofilm contains a higher concentration of redox-active molecules, such as DNA, proteins, metabolites and other electron carrier components of EPS, which enhance the biofilm's intrinsic electrochemical conductivity. Moreover, the close spatial arrangement of cell aggregates could promote efficient electron-transfer pathways between surface-attached cells and the electrode. It was previously shown that the accumulation of redox-active components facilitates both intercellular and electrode-mediated electron transport, thereby decreasing the interfacial resistance.[32−34] Such dynamic evolution could explain the observed decrease in R_{ct} values over time, reflecting the progressive electrochemical integration and functional maturation of the biofilm.[35,36]

To verify whether the *B. cereus* cell community formed on the ITO surface was more structured and metabolically optimized than within the biofilms on gold, we performed microscopic analyses. Both CLSM and SEM showed that the 24 h *B. cereus* biofilm on ITO contained numerous planktonic cells embedded within a compact biofilm structure and exhibited almost no fiber-like structures (Figure 4). In contrast to the biofilm on the gold electrode, the biofilm on ITO was only weakly labeled with PI, indicating lower extracellular DNA production and fewer dead cells (Figure 4a). The ITO surface was almost uniformly covered with densely associated, metabolically active sessile cells (Figure 4b and Figure S3), consistent with our electrochemical measurements. Finally, to determine whether, like on a gold surface, *B. cereus* cells in direct contact with the ITO surface, produced fiber-like structures, we fixed and washed the biofilm before the SEM imaging. This procedure removed the upper biofilm layers and revealed individual planktonic cells attached to the ITO surface, many of which were undergoing division (Figure 4c). Moreover, no bacterial spores were observed on the ITO electrodes at 24 h. All the observed differences in the imaging of biofilms on the two surfaces, ITO and gold, are consistent with the EIS results showing that *B. cereus* biofilm formation is favored on ITO compared to gold. Similarly, a recent study on *E. coli* biofilm growth monitoring using guided wave ultralong-range surface plasmon resonance showed that the growth rate over the SiO_2 surface was higher than on gold, possibly due to differences in surface charge effects.[13] Together, our findings confirm that non-Faradaic impedance enables tracking the functional maturation and electrochemical integration of microbial biofilms.

In conclusion, we report an impedimetric and microscopic characterization of *B. cereus* biofilm dynamics on solid–liquid interfaces. The assays were performed on gold and ITO substrates to monitor electrochemical parameters at different time points. On the gold substrate, a decrease in R_{ct} was observed after 48 h of incubation. Biofilms were visualized by SEM and by live/dead staining followed by CLSM. Microscopic analyses at 24 h biofilms, revealed that biofilm patches on gold contained large fibril-like structures embedded within the EPS matrix, as well as spores within the mature biofilm, while significant portions of the gold surface remained uncovered. This heterogeneous spatial organization is consistent with the high charge transfer resistance, R_{ct}, measured at 24 h. In contrast, *B. cereus* formed compact, densely associated biofilms on the ITO surface, composed largely of metabolically active cells, many of which were dividing at 24 h. The formation of such compact biofilms on ITO correlated with the low R_{ct} and CPE values.

Our study demonstrates the benefits of EIS in monitoring the development of *B. cereus* biofilms on various substrates and under different nutritional conditions. The impedance spectra showed that both the surface properties and the incubation period significantly influence the electrochemical behavior of the

https://doi.org/10.1021/cbmi.5c00271
Chem. Biomed. Imaging XXXX, XXX, XXX–XXX

biofilm. These findings highlight the dynamic nature of biofilm formation and confirm EIS as a robust, nondestructive tool for assessing biofilm growth, organization, and structural maturation. Commercial systems for electrochemical biofilm characterization, such as xCELLigence and DropSens IDE platforms, typically incorporate gold microelectrodes for impedance monitoring. However, our results indicate that the porous gold surface may exert an inhibitory effect on biofilm formation, suggesting that alternative electroactive materials should also be considered for such devices. Finally, while EIS provides a convenient and powerful method for quantifying key electrophysiological features of biofilms, its combined use with high-resolution microscopy provides a comprehensive understanding of biofilm architecture and developmental states.

■ ASSOCIATED CONTENT

Supporting Information

The Supporting Information is available free of charge at https://pubs.acs.org/doi/10.1021/cbmi.5c00271.

Additional experimental details, materials and methods; image of the three-electrode cell; additional SEM images of biofilms (PDF)

■ AUTHOR INFORMATION

Corresponding Author

Jasmina Vidic − *Institut Micalis, INRAE, AgroParisTech, Université Paris-Saclay, 78350 Jouy-en-Josas, France;* orcid.org/0000-0002-8549-8199; Email: jasmina.vidic@inrae.fr

Authors

Aleksandar Mijajlovic − *Faculty of Chemistry, Department of Analytical Chemistry, University of Belgrade, 11158 Belgrade, Serbia*

Dalibor Stankovic − *Faculty of Chemistry, Department of Analytical Chemistry, University of Belgrade, 11158 Belgrade, Serbia;* orcid.org/0000-0001-7465-1373

Milica Sentic − *Institut Micalis, INRAE, AgroParisTech, Université Paris-Saclay, 78350 Jouy-en-Josas, France; Institute of Chemistry, Technology and Metallurgy, National Institute of the Republic of Serbia, University of Belgrade, 11001 Belgrade, Serbia*

Vlad Costache − *Institut Micalis, INRAE, AgroParisTech, Université Paris-Saclay, 78350 Jouy-en-Josas, France; MIMA2, Imaging Core Facility, Microscopie et Imagerie des Microorganismes, Animaux et Aliments, INRAE, 75338 Jouy-en-Josas, France*

Shanshan Wang − *Bordeaux INP, ISM, UMR 5255 CNRS, Site ENSMAC, University of Bordeaux, 33607 Pessac, France*

Hadi Jbara − *Institut Micalis, INRAE, AgroParisTech, Université Paris-Saclay, 78350 Jouy-en-Josas, France*

Julien Deschamps − *Institut Micalis, INRAE, AgroParisTech, Université Paris-Saclay, 78350 Jouy-en-Josas, France*

Romain Briandet − *Institut Micalis, INRAE, AgroParisTech, Université Paris-Saclay, 78350 Jouy-en-Josas, France*

Neso Sojic − *Bordeaux INP, ISM, UMR 5255 CNRS, Site ENSMAC, University of Bordeaux, 33607 Pessac, France;* orcid.org/0000-0001-5144-1015

Complete contact information is available at: https://pubs.acs.org/10.1021/cbmi.5c00271

Notes

The authors declare no competing financial interest.

■ ACKNOWLEDGMENTS

This work was supported by the Agence Nationale de la Recherche (Elise-ANR-21-CE42-009, and Siena ANR-21-CE21-008), the European Union under Grant Agreements No. 101135402 (MOBILES project), and the Program Campus France "Pavle Savic". S.W. and N.S. gratefully acknowledge the support of K. C. Wong Education Foundation and of CNRS. A.M., M.S., and D.S. acknowledge the support of the Ministry of Science, Technological Development and Innovation of the Republic of Serbia, Contract Nos. 451-03-136/2025-03/200026 and 451-03-66/2025-03/200168.

■ REFERENCES

(1) Cormontagne, D.; Rigourd, V.; Vidic, J.; Rizzotto, F.; Bille, E.; Ramarao, N. *Bacillus cereus* induces severe infections in preterm neonates: implication at the hospital and human milk bank level. *Toxins* **2021**, *13* (2), 123.

(2) Pitt, T.; McClure, J.; Parker, M.; Amezquita, A.; McClure, P. *Bacillus cereus* in personal care products: risk to consumers. *International journal of cosmetic science* **2015**, *37* (2), 165−174.

(3) Majed, R.; Faille, C.; Kallassy, M.; Gohar, M. *Bacillus cereus* biofilms—same, only different. *Frontiers in Microbiology* **2016**, *7*, 1054.

(4) Lin, Y.; Briandet, R.; Kovács, Á. T. *Bacillus cereus* sensu lato biofilm formation and its ecological importance. *Biofilm* **2022**, *4*, 100070.

(5) Vidic, J.; Chaix, C.; Manzano, M.; Heyndrickx, M. Food sensing: Detection of *Bacillus cereus* spores in dairy products. *Biosensors* **2020**, *10* (3), 15.

(6) Setlow, P. Spores of *Bacillus subtilis*: their resistance to and killing by radiation, heat and chemicals. *Journal of applied microbiology* **2006**, *101* (3), 514−525.

(7) Verplaetse, E.; Slamti, L.; Gohar, M.; Lereclus, D. Cell differentiation in a *Bacillus thuringiensis* population during planktonic growth, biofilm formation, and host infection. *MBio* **2015**, *6* (3), DOI: 10.1128/mBio.00138-15.

(8) Guzmán-Soto, I.; McTiernan, C.; Gonzalez-Gomez, M.; Ross, A.; Gupta, K.; Suuronen, E. J.; Mah, T.-F.; Griffith, M.; Alarcon, E. I. Mimicking biofilm formation and development: Recent progress in in vitro and in vivo biofilm models. *Iscience* **2021**, *24* (5), 102443.

(9) Auger, S.; Henry, C.; Péchaux, C.; Lejal, N.; Zanet, V.; Nikolic, M. V.; Manzano, M.; Vidic, J. Exploring the impact of Mg-doped ZnO nanoparticles on a model soil microorganism *Bacillus subtilis*. *Ecotoxicology and environmental safety* **2019**, *182*, 109421.

(10) Abouhagger, A.; Celiešiūtė-Germanienė, R.; Bakute, N.; Stirke, A.; Melo, W. C. Electrochemical biosensors on microfluidic chips as promising tools to study microbial biofilms: a review. *Frontiers in Cellular and Infection Microbiology* **2024**, *14*, 1419570.

(11) Pinamonti, D.; Manzano, M.; Maifreni, M.; Bianco, S.; Domi, B.; Ferrin, A.; Anba-Mondoloni, J.; Dechamps, J.; Briandet, R.; Vidic, J. Prevalence and characterization of *Staphylococcus aureus* isolated from meat and milk in Northeastern Italy. *Journal of Food Protection* **2025**, *88* (2), 100442.

(12) Salazar, J.; Amer, M.-À.; Turó, A.; Castro, N.; Navarro, M.; Soto, S.; Gabasa, Y.; López, Y.; Chávez, J.-A. Real-time detection of the bacterial biofilm formation stages using QCM-based sensors. *Chemosensors* **2023**, *11* (1), 68.

(13) Bajaj, A.; Abutoama, M.; Isaacs, S.; Abuleil, M. J.; Yaniv, K.; Kushmaro, A.; Modic, M.; Cvelbar, U.; Abdulhalim, I. Biofilm growth monitoring using guided wave ultralong-range Surface Plasmon Resonance: A proof of concept. *Biosens. Bioelectron.* **2023**, *228*, 115204.

(14) Nguyen, C. Q.; Thrift, W. J.; Bhattacharjee, A.; Ranjbar, S.; Gallagher, T.; Darvishzadeh-Varcheie, M.; Sanderson, R. N.; Capolino, F.; Whiteson, K.; Baldi, P.; et al. Longitudinal monitoring of biofilm formation via robust surface-enhanced Raman scattering quantification

of *Pseudomonas aeruginosa*-produced metabolites. *ACS Appl. Mater. Interfaces* **2018**, *10* (15), 12364−12373.
(15) Lecadet, M.-M.; Blondel, M.-O.; Ribier, J. Generalized transduction in *Bacillus thuringiensis* var. berliner 1715 using bacteriophage CP-54Ber. *Microbiology* **1980**, *121* (1), 203−212.
(16) Agilent. xCELLigence Real-Time Cell Analyzers. 2017.
(17) Kim, T.; Kang, J.; Lee, J.-H.; Yoon, J. Influence of attached bacteria and biofilm on double-layer capacitance during biofilm monitoring by electrochemical impedance spectroscopy. *Water research* **2011**, *45* (15), 4615−4622.
(18) Lazanas, A. C.; Prodromidis, M. I. Electrochemical impedance spectroscopy − a tutorial. *ACS measurement science au* **2023**, *3* (3), 162−193.
(19) Ciucci, F. Modeling electrochemical impedance spectroscopy. *Current Opinion in Electrochemistry* **2019**, *13*, 132−139.
(20) Zhang, J.; Wang, S.; Ono, K. Electrochemical impedance spectroscopy. In *Microscopy and Microanalysis for Lithium-Ion Batteries*; CRC Press, 2023; pp 301−350.
(21) Dheilly, A.; Linossier, I.; Darchen, A.; Hadjiev, D.; Corbel, C.; Alonso, V. Monitoring of microbial adhesion and biofilm growth using electrochemical impedancemetry. *Applied microbiology and biotechnology* **2008**, *79* (1), 157−164.
(22) Grassi, F.; Cums, C.; Cuypers, D.; Verplancke, R.; Vackier, T.; Schaubroeck, D.; Van Haeverbeke, M.; Steenackers, H.; Op de Beeck, M. Sputtered Iridium Oxide Electrodes Optimization and Implementation for Impedimetric Identification of *S. aureus* and *P. aeruginosa* Biofilms. *J. Electrochem. Soc.* **2025**, *172* (3), 035501.
(23) Akabuogu, E. U.; Zhang, L.; Krasovec, R.; Roberts, I. S.; Waigh, T. A. Electrical impedance spectroscopy with bacterial biofilms: neuronal-like behavior. *Nano Lett.* **2024**, *24* (7), 2234−2241.
(24) Kim, I. H.; Shin, J. H.; Jeong, S. B.; Hwang, G. B.; Park, C. W.; Jung, J. H. Compact and Cost-Effective Autofluorescence Sensor for Real-time Environmental Biofilm Monitoring. *Environ. Res.* **2025**, *283*, No. 122171.
(25) Mountcastle, S. E.; Vyas, N.; Villapun, V. M.; Cox, S. C.; Jabbari, S.; Sammons, R. L.; Shelton, R. M.; Walmsley, A. D.; Kuehne, S. A. Biofilm viability checker: An open-source tool for automated biofilm viability analysis from confocal microscopy images. *npj Biofilms and Microbiomes* **2021**, *7* (1), 44.
(26) Arnaouteli, S.; Bamford, N. C.; Stanley-Wall, N. R.; Kovács, Á. T. *Bacillus subtilis* biofilm formation and social interactions. *Nature Reviews Microbiology* **2021**, *19* (9), 600−614.
(27) Virdis, B.; Millo, D.; Donose, B. C.; Lu, Y.; Batstone, D. J.; Krömer, J. O. Analysis of electron transfer dynamics in mixed community electroactive microbial biofilms. *Rsc Advances* **2016**, *6* (5), 3650−3660.
(28) Jain, A.; Gazzola, G.; Panzera, A.; Zanoni, M.; Marsili, E. Visible spectroelectrochemical characterization of *Geobacter sulfurreducens* biofilms on optically transparent indium tin oxide electrode. *Electrochim. Acta* **2011**, *56* (28), 10776−10785.
(29) Naradasu, D.; Miran, W.; Okamoto, A. Electrochemical characterization of two gut microbial strains cooperatively promoting multiple sclerosis pathogenesis. *Microorganisms* **2024**, *12* (2), 257.
(30) Wang, H.; Long, X.; Sun, Y.; Wang, D.; Wang, Z.; Meng, H.; Jiang, C.; Dong, W.; Lu, N. Electrochemical impedance spectroscopy applied to microbial fuel cells: A review. *Frontiers in microbiology* **2022**, *13*, 973501.
(31) Romero Serrano, M. C.; Méndez-Tovar, M. Impedance Analysis for the Study of Biofilm Formation on Electrodes: An Overview. *Journal of the Mexican Chemical Society* **2023**, *67* (4), 547−565.
(32) González, T.; Ureta-Zañartu, M.; Marco, J. F.; Vidal, G. Effect of Zeolite-Fe on graphite anode in electroactive biofilm development for application in microbial fuel cells. *Appl. Surf. Sci.* **2019**, *467*, 851−859.
(33) Baranitharan, E.; Khan, M. R.; Prasad, D.; Teo, W. F. A.; Tan, G. Y. A.; Jose, R. Effect of biofilm formation on the performance of microbial fuel cell for the treatment of palm oil mill effluent. *Bioprocess Biosyst. Eng.* **2015**, *38* (1), 15−24.
(34) Borole, A. P.; Aaron, D.; Hamilton, C. Y.; Tsouris, C. Understanding long-term changes in microbial fuel cell performance using electrochemical impedance spectroscopy. *Environ. Sci. Technol.* **2010**, *44* (7), 2740−2745.
(35) Hirsch, L. O.; Gandu, B.; Chiliveru, A.; Dubrovin, I. A.; Jukanti, A.; Schechter, A.; Cahan, R. Hydrogen Production in Microbial Electrolysis Cells Using an Alginate Hydrogel Bioanode Encapsulated with a Filter Bag. *Polymers* **2024**, *16* (14), 1996.
(36) Cai, T.; Zhang, Y.; Wang, N.; Zhang, Z.; Lu, X.; Zhen, G. Electrochemically active microorganisms sense charge transfer resistance for regulating biofilm electroactivity, spatio-temporal distribution, and catabolic pathway. *Chemical Engineering Journal* **2022**, *442*, 136248.

https://doi.org/10.1021/cbmi.5c00271
Chem. Biomed. Imaging XXXX, XXX, XXX−XXX